SEMARAK ILMU PUBLISHING

CFD Letters

Journal homepage:
https://semarakilmu.com.my/journals/index.php/CFD_Letters/index
ISSN: 2180-1363

Numerical Investigation of Variation Stroke Plane Effect on Aerodynamic Performance of a 2D Flapping Airfoil Naca 0012 in Hovering Flight

Mohamed El Amine Trifi[1], Redha Rebhi[2,*] Abdellah Abdellah Elhadj[1], Shayfull Zamree Abd Rahim[3,4]

[1] Laboratoire de Mecanique Physique et Modelisation Mathematique, University of Medea, Medea, Algeria
[2] Department of Mechanical Engineering, Faculty of Technology, University of Medea, Medea, Algeria
[3] School of Manufacturing Engineering, Universiti Malaysia Perlis, Main Campus Pauh Putra, 02600 Arau, Perlis, Malaysia
[4] Green Design and Manufacture Research Group, Center of Excellence Geopolymer and Green Technology (CEGeoGTech), Universiti Malaysia Perlis, 01000 Kangar, Perlis, Malaysia

ARTICLE INFO

Article history:
Received 24 May 2022
Received in revised form 13 July 2022
Accepted 28 July 2022
Available online 31 August 2022

Keywords:
Inclined stroke plane; Hovering flight; Aerodynamic characteristics; Energy consumption; Reynolds number; Oscillation amplitude

ABSTRACT

This paper presents a numerical study of the effects generated by the variation of translation plane inclination angle on the aerodynamic performance (aerodynamic forces, energy consumption, and wing flow structures). This inclination angle is called β (such as $90° \leq \beta \leq 0°$). In our work, a two-dimensional NACA0012 airfoil will be presented using Ansys Fluent commercial software based on the finite volumes method (FVM).The numerical simulations are carried out using the experimental results parameters. Symmetric wing flapping motions with different angles of the stroke plane inclination β in conjunction with other kinematic parameters such as oscillation amplitude ($15° \leq \Delta\alpha \leq 45°$) and Reynolds number ($1.35.10^5 \leq Re \leq 1.35$) are examined to investigate the influence of these parameters on the energy consumption of the NACA0012 profile. The governing parameters of the problem under study are: the chord of the profile C, the initial angle of rotation α_0 , the oscillation amplitude $\Delta\alpha$, the reduced frequency k, Reynolds number $Re = 1.35 \times 10^5$, flow velocity U_∞ , turbulence intensity at the inlet is 0.08%, translation amplitude A_m and phase difference between the rotation and translation motion φ .The obtained numerical results were compared with the experimental data. Moreover, vorticity and pressure contours for different values of angle β will be also presented.

1. Introduction

The flight of insects always arouses astonishment: take-off in backward flight, landing on the back of a leaf, hovering or fluttering in all kinds of ways. Their unequalled aerial performances remained unexplained for a long time, because of their small size. It took the development of imaging and computational techniques to gradually understand how insects fly.

Understanding the fundamental mechanisms of insect flight is crucial in practical applications for the design of micro air vehicles (MAVs) and wind turbines. In recent years, many numerical and

* *Corresponding author.*
E-mail address: rebhi.redha@gmail.com (Rebhi Redha)

https://doi.org/10.37934/cfdl.14.8.8199

experimental studies have been conducted to investigate the aerodynamic performance of insects, these studies mainly focus on thrust generation at different pitch and dive frequencies and on the improvement of lift characteristics, flow development and leading-edge vortex (LEV) dynamics in flapping motion.

Ahmad *et al.,* [1] performed numerical simulations to investigate the effect of different mesh parameters for accurately estimating the drag of a ground vehicle. A simplified car model at three scales has been investigated and compared with results from the MIRA model wind tunnel. This study shows that with mesh optimization it is possible using a PC to make accurate predictions of the drag coefficient within 4% of the wind tunnel measured value. Abobaker *et al.,* [2] numerically investigated the effect of structured and unstructured mesh types on lift and drag coefficients. The numerical results show that at the linear aerodynamic range, i.e. up to 8 degrees, structured and unstructured grid follow experimental data with the same accuracy. For angles of attack higher than 8 degrees, the unstructured mesh overestimates the experimental lift coefficient, while structured grid results are closer to experimental data.

Abdulameer Shlash and Koç [3] investigated the flow and heat transfer of turbulent fluid flow through channels with various vortex generator designs mathematically (triangular, half-circle, and quarter circle) and the effect of geometrical factors such as step height (2, 3, 4, 5, and 6 mm) on the flow and heat fields. The results showed that the skin friction coefficient and the surface Nu rise with step height and reach their maximum value at 4 mm, according to the findings. Furthermore, as the Re increases, so does the average Nu sum. At a step height of 4 mm, the quarter circle VG outperforms the triangular VG in terms of thermal-hydraulic efficiency. The simulation results conform well with those in the literature. Alias *et al.,* [4] studied the effects of the gap ratio (G/D) of a drilling riser with auxiliaries on the vortex shedding phenomenon on a fixed and freely vibrating riser. The results show that the freely vibrating riser experienced higher lift and drag forces compared to the fixed riser due to high frequencies of hydrodynamics forces fluctuations on the main cylinder.

Wernert *et al.,* [5] studied experimentally and numerically, the deep dynamic stall of a $\mathrm{NACA0012}$ airfoil in pitch, the comparison between experimental and numerical results was conducted for the deep dynamic stall process which was studied in a low-speed open wind tunnel using PIV, laser sheet visualizations and $\mathrm{Navier-Stokes}$ calculations, and the computational results were in agreement with the experimental results. Anderson *et al.,* [6] showed that high efficiency accompanied by thrust development is associated with the generation of moderately strong leading-edge vortices, which then merge with the leading-edge vortices and amalgamate with the trailing edge vorticity leading to the formation of an inverted Karman vortex. Lee and Gerontakos [7] studied an experimental analysis of the boundary layer characteristics and stall phenomena developing on a $\mathrm{NACA\ 0012}$ oscillating profile at $Re = 1{,}35 \times 10^5$ where small values of reduced frequency were required to delay the onset of the various boundary layer events and to produce significant variations in the amplitude of the C_L, C_D, and C_M peaks. Wang *et al.,* [8] study numerically the fluid flow around two sinusoidal pitch $\mathrm{NACA0012}$ airfoils in low Reynolds number regime ($Re = 10^5$), with varying frequencies and by using two URANS models such as the standard $\mathrm{k-\omega}$ model and the $\mathrm{k-\omega\ SST}$ model with transition. The results are compared to experimental data where the $\mathrm{k-\omega\ SST}$ model performs well and shows improvement over the standard $k-\omega$ model and also the $\mathrm{k-\omega\ SST}$ model can predict experimental data with reasonable accuracy.

Amiralaei *et al.,* [9-11] investigated the effects of unsteady flow and system's parameters $(d, k \text{ and } Re)$ on the instantaneous force coefficients and flow patterns on a $\mathrm{2D}$ flow around a $\mathrm{NACA0012}$ profile performing dynamic pitching motion at low Reynolds number (less than 5000). The results show the substantial influence of the above-mentioned unsteady parameters on the maximum lift and drag coefficients, these three parameters $(d, k, \text{and } Re)$are important for the

aerodynamic characteristics. A higher reduced frequency widens the area of the hysteresis curves and increases the maximum value of the lift coefficients. The change in amplitude generated a difference in aerodynamic forces for the same angle of attack. At higher amplitude, strong leading and trailing edge vortex effects occurred. Bhat and Govardhan [12] experimentally investigated the limits of stall flutter of a low Reynolds number NACA 0012 airfoil by measuring the forces and flow fields around the airfoil when forced to oscillate. These measurements indicated that for large average angles of attack of the airfoil, there is a positive energy transfer to the airfoil over a reduced frequency range, indicating that there is a possibility of airfoil excitation or stall flutter. Liu *et al.,* [13] investigated numerically the performance of aerodynamic profiles in pitch at high amplitudes. The pitching motion delayed the initial incidence of the LEV, thereby enhancing the flutter. The amplitude enhanced the maximum lift and stall incidence and had a significant effect on the hysteresis. Zakaria *et al.,* [14,15] investigated experimentally the flow field and lift enhancement of an NACA0012 airfoil subjected to dipping oscillations and proposed a frequency response method to predict the unsteady aerodynamics of dipping oscillations of an airfoil. The results show that the increase in lift is caused by the vortices coming off the leading edge. The lift amplitude was increased beyond the stall regime when the reduced frequency was 0.7.

Sun and Tang [16] developed a computational model to examine the flapping motion of a fruit fly in normal stationary flight mode. The problem is treated by solving numerically the Navier-Stokes equations. This study indicated that rapid acceleration or rotation has a strong influence on the instantaneous lift peaks that increase with higher translational velocity or rotation. Wang *et al.,* [17] studied the comparison of two-dimensional (2D) calculations and three-dimensional (3D) experiments of a hovering wing undergoing sinusoidal motion along a horizontal stroke plane in several qualitatively different kinematic models. In all cases, the calculated drag compares well with the experiments. The calculated lift agrees in cases where the sinusoidal changes of the angle of attack are symmetrical or advanced with respect to the experiments. But the results show that there is no significant difference in force generation between the two-dimensional calculation and the three-dimensional experiment. These numerical results suggest that three-dimensional simulations are not necessarily necessary to explain the high lift generated during hovering.

Meile *et al.,* [18] investigated experimentally and numerically the aerodynamic behaviour of the Ahmed body with two different rearslant angles was investigated by wind tunnel experiments and numerical simulations. one part of the study was focused on wind tunnel experiments to provide reliable data on forces and moments at the same Reynolds number. The simulation results are in good agreement with the measurements for symmetrical flow in both cases of the slant angle, especially for the drag. Wang [19] studied the unsteady aerodynamics of two-dimensional wing flapping in insect hovering with an inclined plane by solving the Navier-Stokes equations, the results showed that two-dimensional hovering motion can generate sufficient lift to support the weight of an insect. Yu and Tong [20] investigated theoretically the effects of asymmetric durations of the down stroke and upstroke in inclined forward flight to understand the physics of insect flows. The results indicate that the asymmetric stroke with longer down stroke duration generates more thrust but changes the lift and aerodynamic input power little. Gao and Lu [21] studied normal insect hovering with a ground effect on unsteady forces and vortex structures, the goal of this study is to provide physical insight for understanding the aerodynamics and flow structures for normal insect hovering. Jardin *et al.,* [22] investigated experimentally the effects of asymmetric flapping on wing motions during inclined hovering. Asymmetry was introduced by differentiating between down stroke and upstroke angles of attack. It was found that asymmetric flapping motions in inclined hovering were particularly more efficient than normal flapping motions in hovering with horizontal plane of attack. Sudhakar and Vengadesan [23] revealed the influence of kinematic parameters (Re, stroke

amplitude, rotation timing and rotation duration) on force production of inclined hovering stroke. The study focused on the influence of the aforementioned parameters on the unsteady aerodynamic mechanisms of insect flight, namely delayed stall, rotational circulation, wake capture and added mass. Furthermore, the significance of the study is Re that indicates that the proposed asymmetric hovering mechanism for small insects may not work. Shanmugam and Sohn [24] conducted a systematic study of a flapping wing in inclined plane hover for several parameter spaces: Pitch amplitudes with other kinematic parameters such as stroke plane inclination $(10° \leq \beta \leq 80°)$, stroke amplitude$(0.5 \leq Ao/c \leq 5)$, heave-pitch phase difference$(-45° \leq \varphi \leq 90°)$, and Reynolds number $(15.7 \leq Re \leq 10^4)$ on the aerodynamic performance and vortex structures. The results indicate that the pitch magnitude B has a significant effect on the aerodynamic performance.

Abdul Aziz *et al.,* [25] numerically investigated the power from micro hydropower generation through conical gravitational water vortex turbine (GWVT) via SOLIDWORKS flow simulation. Two different turbine orientations were simulated i.e., vertical and horizontal at different blade angle designs i.e., 25°, 45°, 75°, 90°, and 120° and with different number of blades i.e., 8, 12, and 18 while forces were harnessed at tangential (z-axis) direction. The simulation results showed that it was possible to run and produce force from conical GWVT design in a fully enclosed system. It was found that vertical turbine orientation produced a slightly higher force than horizontally orientated turbine, using 12 runner blades at 90° angles where the distributed forces were 15.31N and 14.12N respectively, at tangential (z-axis) direction. Rival *et al.,* [26] investigated experimentally and numerically the energy recovery of leading edge vortices (LEV) and trailing edge vortices (TEV) in a tandem blade configuration at $Re = 3 \times 10^5$ and $k = 0.25$. For phase differences of $0°$, $30°$ and $60°$, a normal force was generated during the upstroke, which helped to reduce energy consumption.

In this paper, we use a numerical model to study the flapping motion of an $\mathrm{NACA0012}$ airfoil, the main objective is to evaluate the effect of varying the inclined stroke-plane hovering along the angle β on the behavior of forces (lift, moment and energy coefficients) and the flow around an $\mathrm{NACA0012}$ airfoil. Based on the experimental parameters chosen from $\mathrm{Lee\ and\ Gerontakos}$ [3], the flow around the $\mathrm{NACA0012}$ airfoil is solved in two dimensions using the industry code $\mathrm{CFDANSYS\ Fluent16.2}$. By comparing the simulation results, it is possible to determine the optimal angle of the inclined stroke plane β to improve the hovering efficiency of the NACA0012 profile in flapping motion.

2. Numerical Simulation Methodology

2.1 Numerical Method and Mathematical Formulation

The governing equations to study the flapping motion and the flow around an aerodynamic profile NACA0012 (as shown in figure 1) are the two-dimensional $\mathrm{Navier-Stokes}$ equations and they are given by the following relations:

$$\frac{\partial u}{\partial t} + u\,.\nabla u = -\frac{1}{\rho}\nabla p + v\nabla^2 u \tag{1}$$

$$\nabla\,.u = 0 \tag{2}$$

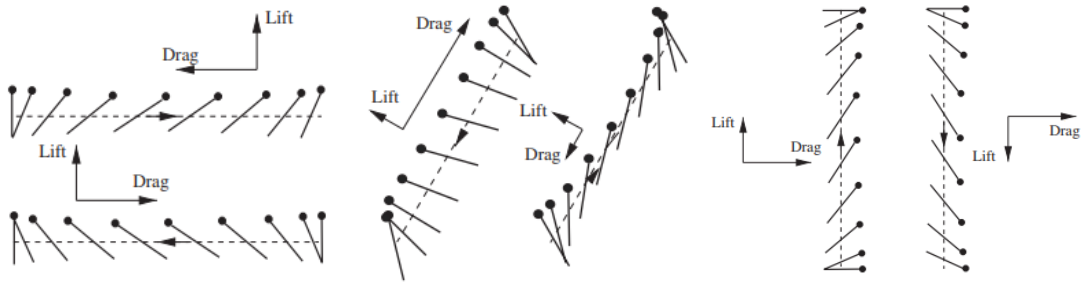

Fig. 1. Diagram of the wing movement

The ANSYS Fluent 16.2 fluid dynamics solver was used to simulate the aerodynamic forces and flow fields under constant free-flow velocity with different unsteady and kinematic parameters. The governing equations were discretized based on the finite volume method. The standard $\mathrm{k}-\omega$ turbulence model was chosen, due to the incompressible flow, the pressure-based Navier $-$ Strokes solution algorithm was chosen and the Semi-Implicit Method for Pressure Linked Equations Consistent (SIMPLEC) algorithm was applied for the pressure-velocity coupling, while a second-order scheme was used for the spatial discretization of the simulations performed. The convergence criteria for the residuals were 10^{-3}.

The geometry and kinematics of the flapping airfoil in hovering flight on the horizontal, inclined and vertical planes are illustrated in Figure 1.

In particular, the flapping motion of the airfoil is combined with a translation and a rotation in a stroke plane with an angle of inclination that can be described as follows:

$$A(t) = A_m \cos(2\pi f t)(cos\beta, sin\beta) \tag{3}$$

$$\alpha(t) = \alpha_0 + \Delta\alpha(2\pi f t + \varphi) \tag{4}$$

where $A(t)$ and $\alpha\ (t)$ are the translational displacement and rotation angle respectively, f is the frequency, the chord length of the airfoil is c, A_m and $\Delta\alpha$ are the translational and rotational amplitudes, respectively, φ is the phase difference between the translation and rotation motion, α_0 is the initial mean angle of attack, time is t, and β is the inclination angle of the stroke plane. The translational velocity is simply a harmonic function of time and the rotation occurs around the geometric center of rotation which is at the point $0.25c$ from the leading edge of the profile.

To identify the characteristics and shape of the fluid flow around a hovering profile, there are mainly two dimensionless parameters, namely the Reynolds number and the reduced frequency, the Reynolds number is defined as follows:

$$Re = \frac{\rho\, U_{ref}\, c}{\mu} \tag{5}$$

where ρ is the density of the fluid$[Kg/m^3]$, c is the chord length of the profile $[m]$, μ is the dynamic viscosity of the fluid $[Kg/m.s]$ and U_{ref} is the reference velocity $[m/s]$ which is defined as the maximum translational speed of the wing:

$$U_{ref} = \frac{2\pi A_m}{T} \tag{6}$$

where $T = \frac{1}{f}$ is the flapping period.

The reduced frequency is defined as follows:

$$K = \frac{\pi f c}{U_{ref}} \tag{7}$$

where f is the flapping frequency.

The components of the force on the profile are calculated by:

$$C_L = \frac{F_L}{0.5\rho {U_{ref}}^2 c}, \quad C_D = \frac{F_D}{0.5\rho {U_{ref}}^2 c}, \quad C_M = \frac{M_Z}{0.5\rho {U_{ref}}^2 c^2} \tag{8}$$

where F_L , F_D and M_Z are the lift, drag and momentum forces respectively.

The energy consumption is determined by:

$$P(t) = -\left[F_{flap} \,.\, \dot{A}(t) + M \,.\, \dot{\alpha}(t)\right] \tag{9}$$

where F_{flap} is the resultant of the flapping force in the stroke direction, $\dot{A}(t)$ is the translation velocity, M is the rotation moment with respect to the pitch point and $\dot{\alpha}(t)$ the rotation velocity of the airfoil.

The energy coefficient is defined by:

$$E_C = \frac{P(t)}{0.5\rho {U_{ref}}^3 c} \tag{10}$$

2.2 Mesh Generation and Boundary Condition

The computational domain used for the simulations has a circular shape as shown in Figure 2 and contains an inner zone called $\Omega 1$ of $20c$ diameter of the profile rotation points and an outer zone $\Omega 2$ of $25c$ diameter. A mesh of structured quadrilateral cells are used in the inner area $\Omega 1$ to encompass all the motion of the profile which moves according to the predefined Eqs. (3) and (4) with user-defined functions (UDF) witch are developed and attached to the Fluent solver to control the dynamic motion of the mesh., while a mesh of unstructured triangular cells are used in the outer $\Omega 2$ area to meet the requirement of remeshing the grid at each time step, with a velocity input as a boundary condition at T_1 and no pressure gradient at the T_2 output.

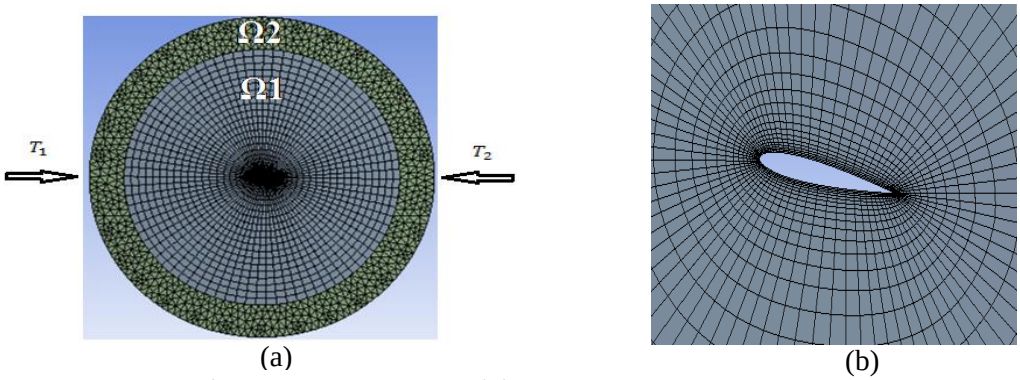

(a) (b)

Fig. 2. Diagram of the model geometry: (a) the boundaries around the computational domain, (b) the close-up view of the mesh near the wing surface

2.3 Validation of CFD Solver

To examine the efficiency and reliability of the numerical code, a pitch oscillation motion of the NACA0012 airfoil was calculated. This pitching motion was governed by the sinusoidal equation: $\alpha(t) = 10^{\circ} + 15^{\circ}(2\pi f t + \varphi)$ with a reduced frequency of $k = 0.05$, the Reynolds number of $Re = 1.35 \times 10^5$, the flow velocity $U_\infty = 14\ m/\mathrm{s}$, the pitch axis is located $0.25c$ from the leading edge, and the rate of inlet turbulence intensity is 0.08%. The $\mathrm{standard\ k-\omega}$ turbulence model was applied. The obtained numerical results were compared with the experimental data of Lee and Gerontakos [3]. The computational results presented in Figures 3(a) and (b) are in agreement with the experimental results for both lift and drag coefficients.

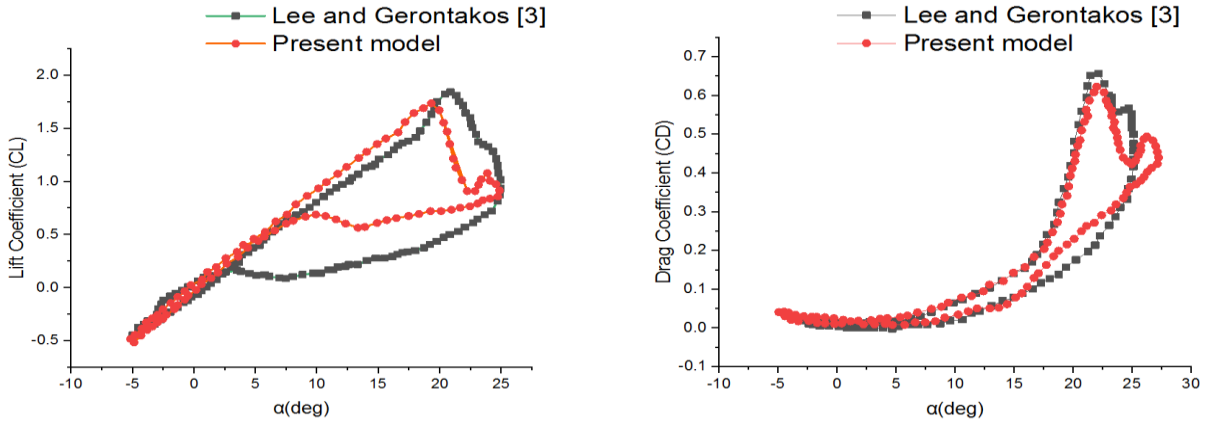

(a) (b)

Fig. 3. (a) Validation of the lift coefficient (CL) according to the angle of attack (b) Validation of the drag coefficient (CD) according to the angle of attack

3. Results and Discussion

3.1 Effect of Plane B

The present study is carried out to evaluate the effects the translational stroke plane variation along the angle β on the force behavior (lift, moment and energy coefficients) and flow around an $\mathrm{NACA0012}$ airfoil in hovering. This study based on the experimental parameters chosen by Lee and Gerontakos [3], the parameters used here are given as follows: the chord of the profile $c = 0.15\mathrm{cm}$, the initial angle of rotation $\alpha_0 = 10°$, the oscillation amplitude Δα=15°, the reduced frequency $k = 0.05$, Reynolds number $Re = 1.35 \times 10^5$, flow velocity $U_\infty = 14\mathrm{m/s}$, turbulence intensity at the inlet is 0.08%, translation amplitude $A_m = 3c$ and phase difference between the rotation and translation motion $\varphi = 0$.

In this case two special cases were studied:

I. The first case, where $\beta \in [90°, 50°]$ corresponds to hovering along a vertical plane ($\beta = 90°$) and an inclined stroke plane similar to dragonfly wing motion;
II. The second case, where $\beta \in [45°, 0°]$ corresponds to hovering along an inclined stroke plane and a horizontal plane ($\beta = 0°$).

3.1.1 Effect of plane in the Case B *∈[90°, 45°]*

We present in Figure 4(a), the time traces of the lift coefficient (C_L) at five different β angles where $\beta = 90°, 80°, 70°, 60°$, and $50°$.It is observed that there is an influence of β on the maximum and minimum peaks of the lift coefficient(C_L), in which the maximum lift coefficient C_{Lmax} and

minimum lift coefficient C_{Lmin} increases as the increase of β except for the case where the value of maximum lift coefficient C_{Lmax} of β=90° is lower than the value of maximum lift coefficient C_{Lmax} of $\beta = 70°$. It can be seen that the change of β has a significant impact on the lift coefficient.

The effects of β on Cl_{max} and $\mathrm{cl_{min}}$ are presented in Table 1, which shows that the variation of both coefficients Cl_{max} and Cl_{min} are higher.

Table 1
Summary of the effect of β on the maximum and minimum lift coefficients

Lift Coefficient	$\beta = 90°$	80°	70°	60°	50°
C_{Lmax}	1.20703	1.23246	1.21793	1.16291	1.09113
C_{Lmin}	0.84399	0.73389	0.65759	0.62609	0.6162

The variation of moment coefficient (C_M) as a function of time is non-sinusoidal in the cases of $\beta = 90°$ and $\beta = 80°$, while it is almost sinusoidal in the cases of $\beta = 70°$, $60°$ and $50°$, as shown in Figure $4(\mathrm{b})$, and it is noticed that the magnitudes of moment coefficients during the pitching motion increased significantly when decreasing the plane β.

The energy consumption performance of a rotating and translating profile along a plane β is directly related to the variation of C_L and C_M coefficients, as shown in Eq. (9). Figure $5(\mathrm{a})$ shows that the energy transfer coefficient (E_C) as a function of time increases with increasing of β, indicating that the greater inclination of the plane β, the energy consumption is greater.

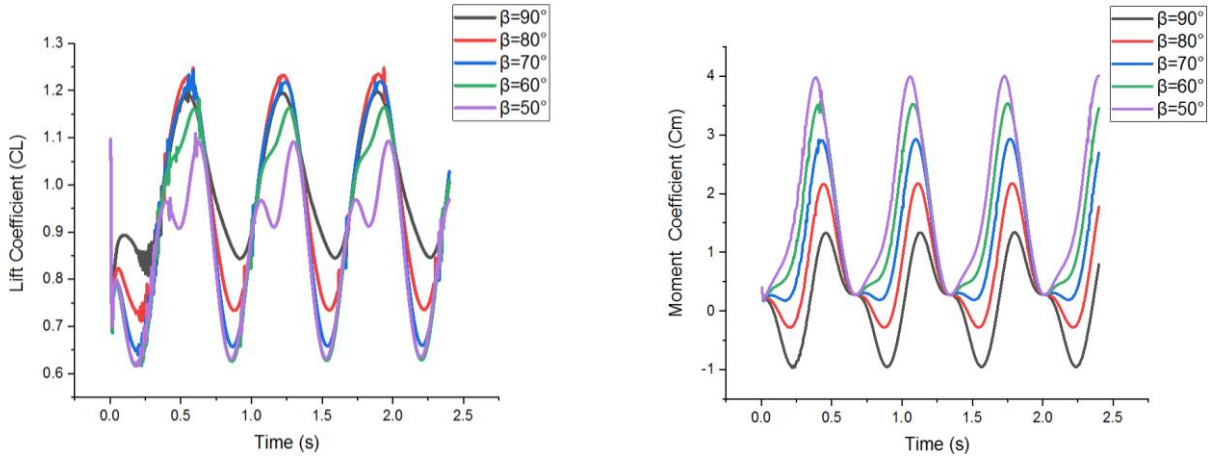

(a) (b)

Fig. 4. (a) Lift coefficient (C_L) as a function of time (s) for cases of β =90°, 80°, 70°, 60° and 50° at the rotation axis 0.25c (b) Moment coefficient (C_M) as a function of time (s) for cases of β =90°, 80°, 70°, 60° and 50° at the rotation axis 0.25c.

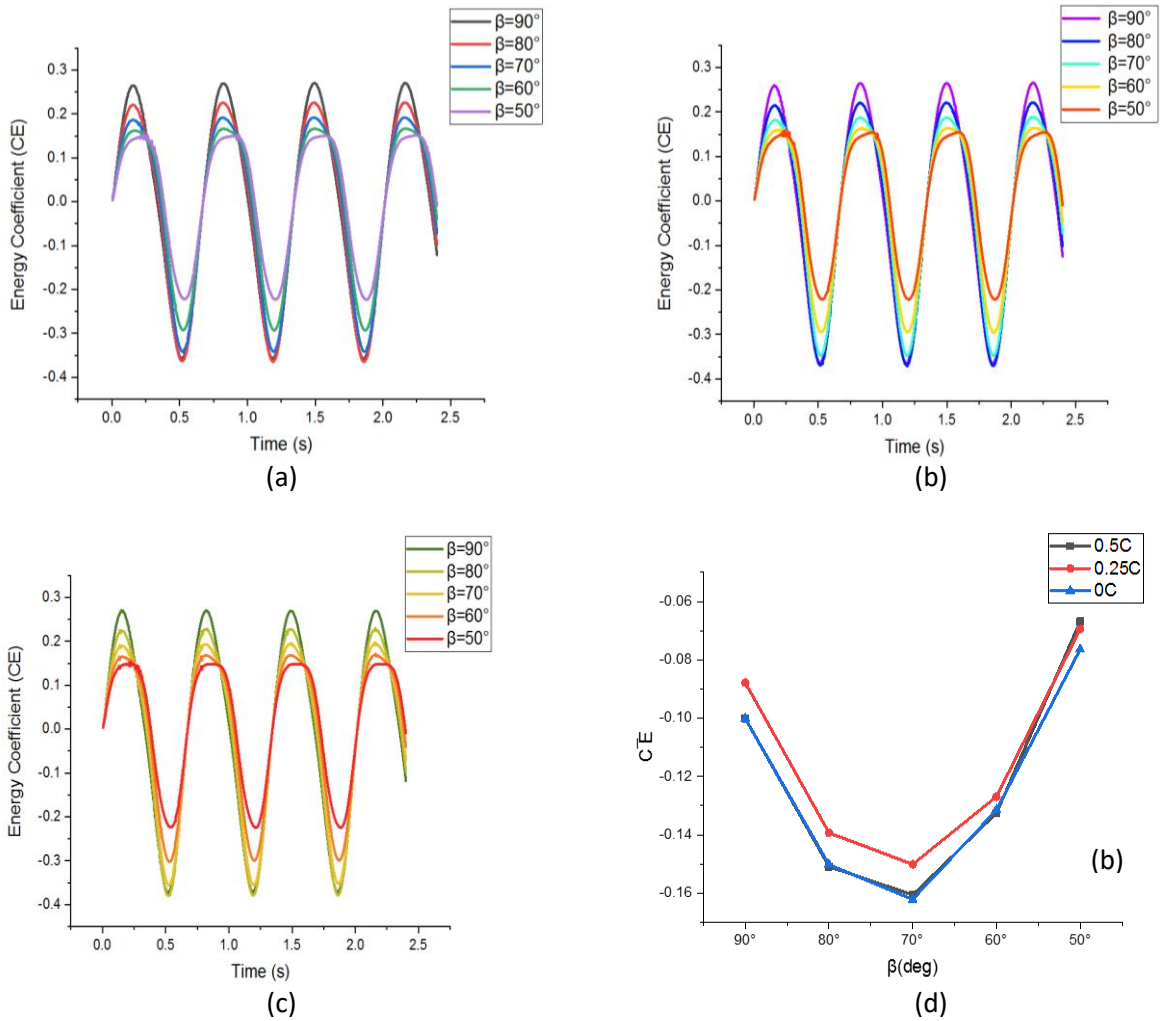

Fig. 5. (a) The time history of energy coefficient (E_C) for the cases of β $= 90°, 80°, 70°, 60°$ and $50°$ at the rotation axis $0.25c$ (b) The time history of energy coefficient (E_C) for the cases of β $= 90°, 80°, 70°, 60°$ and $50°$ at the rotation axis $0.5c$ (c) The time history of energy coefficient (E_C) for the cases of β $= 90°, 80°, 70°, 60°$ and $50°$ at the rotation axis $0.25c$ (d) Average energy coefficient $\overline{(E_C)}$ as a function of β for different axis of rotation at 0.5c, 0.25c and 0c

The effects of β on CE_{max} and CE_{min} are presented in Table 2, which shows that the variation of both coefficients CE_{max} and CE_{min} are higher.

Table 2
Summary of the effect of β on the maximum and minimum energy coefficients

Energy coefficient	β =90°	80°	70°	60°	50°
CE_{max}	0.26956	0.22549	0.19133	0.16587	0.15296
CE_{min}	-0.35737	-0.36484	-0.34147	-0.29278	-0.22242

However, the energy transfer coefficient (E_C) which was shown in Figure $5(a)$, indicates that in each case of β, there are portions of the cycle of the flapping motion of the NACA0012 profile where energy is supplied to the profile $(E_C > 0)$,and parts of the cycle where energy is taken away from the profile $(E_C < 0)$, for which the case of β $= 90°$ is taken, it is evident from this case that the energy coefficient reaches a maximum value E_{Cmax} of 0.26956 at $\alpha = 24.36°$ during the upstroke, and then monotonically decreases to a minimum value E_{Cmin} of -0.35737 at $\alpha = -4.88°$ during

the downstroke, indicating that the maximum energy transfer coefficient E_{Cmax} increases by increasing β while the minimum energy transfer coefficient E_{Cmin} decreases by increasing β.

Furthermore, for the effect of the rotation axis variation of the profile on the energy transfer coefficient (E_C) with the variation of the plane β,we find that the traces of the energy transfer coefficient (E_C) (Figures 5(a)-(c)) for the rotation axes at $0.25c$, $0.5c$ and $0c$ respectively shows the same trend and similar behavior ,as well as, the variation of the energy transfer coefficient (E_C) for the rotation axes at 0.5c and $0c$ is almost identical, but the variation of the energy transfer coefficient (E_C) for the rotation axis at 0.25c was more vary than that of the last two axis, this indicates that the effect of the rotation axis at 0.25c on the variation of the energy transfer coefficient (E_C) is quite obvious than that of the two rotation axis at 0.5c and 0c as can be seen from Table 3.

Table 3
Summary of the effect of β on the maximum and minimum energy coefficients for the rotational axes at 0.5C and 0C

Energy coefficient		β =90°	80°	70°	60°	50°
Axis of rotation: 0.5*c*	CE_{max}	0.26417	0.18676	0.16273	0.15402	0.22014
	CE_{min}	-0.36431	-0.34738	-0.29527	-0.22091	-0.37106
Axis of rotation: 0*c*	CE_{max}	0.27007	0.22861	0.19344	0.16769	0.14782
	CE_{min}	-0.37023	-0.37886	-0.35562	-0.29918	-0.22423

The time-averaged energy transfer $\overline{(E_C)}$ is shown in Figure 5(d), which represents the net energy transfer to the profile, this plot is made to evaluate the effects of the rotational axis location on the average energy coefficient $\overline{(E_C)}$ as a function of β.

Obviously, it was observed from the Figure 5(d) that the average energy coefficient $\overline{(E_C)}$ is completely negative with the three axis of rotation for all values of β (where $\beta = 90°, 80°, 70°, 60°$ and $50°$), and it is observed that the two cases of the axis of rotation that are fixed at 0.5c and 0C of the chord, the average energy coefficient $\overline{(E_C)}$ is strongly negative compared to the first case fixed at 0.25c . In Figure 5(d), it is also observed that the average energy transfer coefficient $\overline{(E_C)}$ gradually decreases with the decrease of β and reaches a minimum value at $\beta = 70°$ and starts to increase strongly reaching its largest value at $\beta = 50°$, and the curves also show that at $\beta = 70°$ the energy consumption (energy which is taken away from the profile) is higher than energies consumption for the other angles such as $\beta = 90°, 80°, 60°$ and $50°$.

3.1.2 Effect of plane in the case $\beta \in [45°, 0°]$

Figure 6(a) represented the lift coefficients (C_L) versus time at six different planes according to β where $\beta = 45°, 40°, 30°, 20°, 10°$, and $0°$. From this graph (Figure 6(a)) it was found that the influence of β on the minimum peaks of the lift coefficient C_{Lmin} is greater than the influence of β on the maximum peaks of the lift coefficient C_{Lmax}, in which the values of the maximum peaks of the lift coefficient C_{Lmax} are almost identical for different values of β, while the values of the minimum peaks of the lift coefficient C_{Lmin} increase more highly by the decrease the values of β.

Figure 6(b) Shows that the variation of moment coefficient (C_M) with time is almost sinusoidal in the cases of $\beta = 45°$ and $\beta = 40°$, while, in the cases of $\beta = 30°, 20°, 10°$ and $0°$ this variation is non-sinusoidal, and it is also noticed that the magnitudes of moment coefficients during the pitching motion decreases significantly when increasing β. The change of the minimum moment coefficient C_{Mmin} was more significant than that of the maximum moment coefficient C_{Mmax}.

The effects of β on Cl_{max} and Cl_{min} are presented in Table 4, which shows that the variation of minimum lift coefficient is higher than that observed for Cl_{max}. Table 4 presented below summarize the effects of angle plane β on the maximum and minimum lift coefficients.

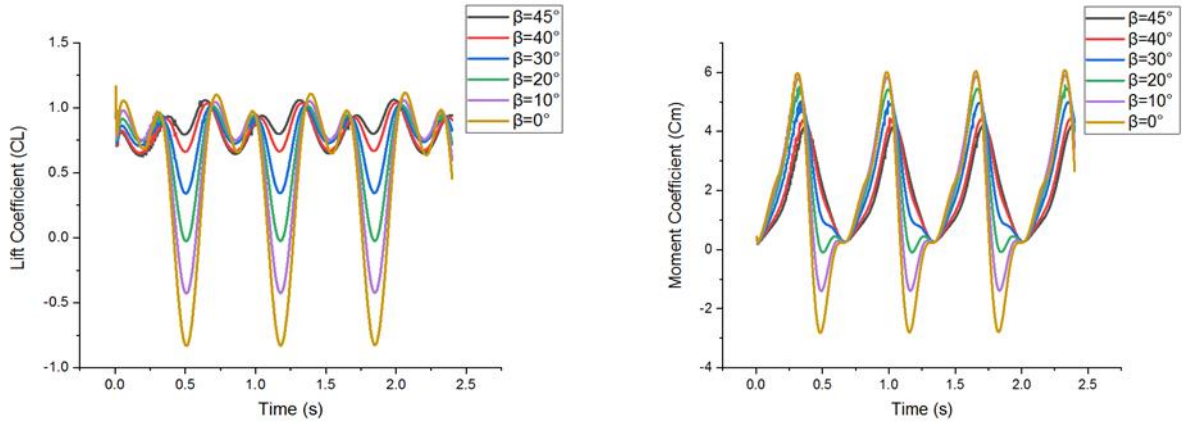

(a) (b)

Fig. 6. (a) Lift coefficient (C_L) as a function of time (s) for cases of β =45°, 40°, 30°, 20° ,10° and 0° at the rotation axis 0.25c (b) Moment coefficient (C_M) as a function of time (s) for cases of β =45°, 40°, 30°, 20° ,10° and 0° at the rotation axis 0.25c

Table 4
Summary of the effect of β on the maximum and minimum lift coefficients

Lift Coefficient	β=45°	30°	40°	20°	10°	0°
C_{Lmax}	1.06096	1.03797	1.01654	1.02027	1.05689	1.11634
C_{Lmin}	0.79833	0.66471	0.34263	-0.02435	-0.42474	-0.82823

The energy transfer coefficient (E_C) as a function of time for the cases of $\beta = 45°, 40°, 30°, 20°, 10°$ and $0°$ with the rotation axis $0.25c$ are shown in $\text{Figure}7(a)$, as observed, it was noticed that the energy transfer coefficient (E_C) increases by the increase of β, which indicates that the effect of plane β on energy consumption is more significant and noticeable.

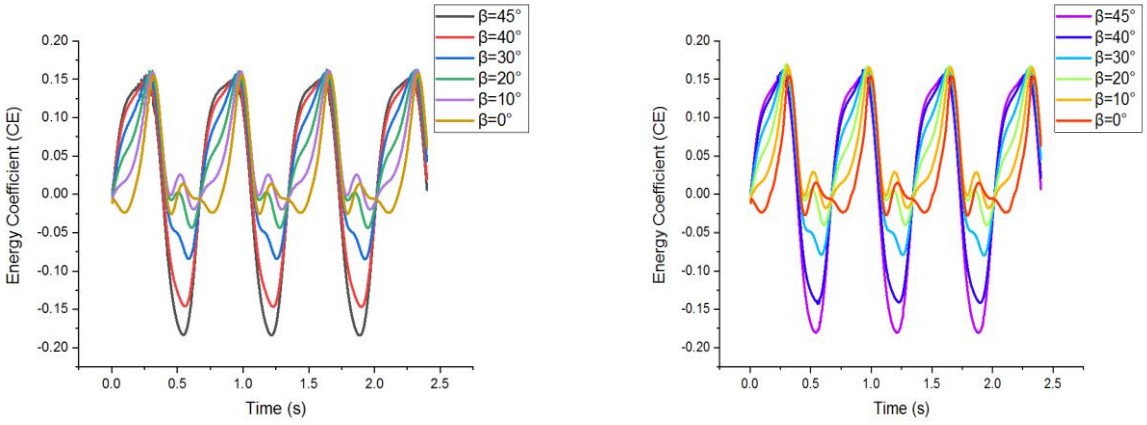

(a) (b)

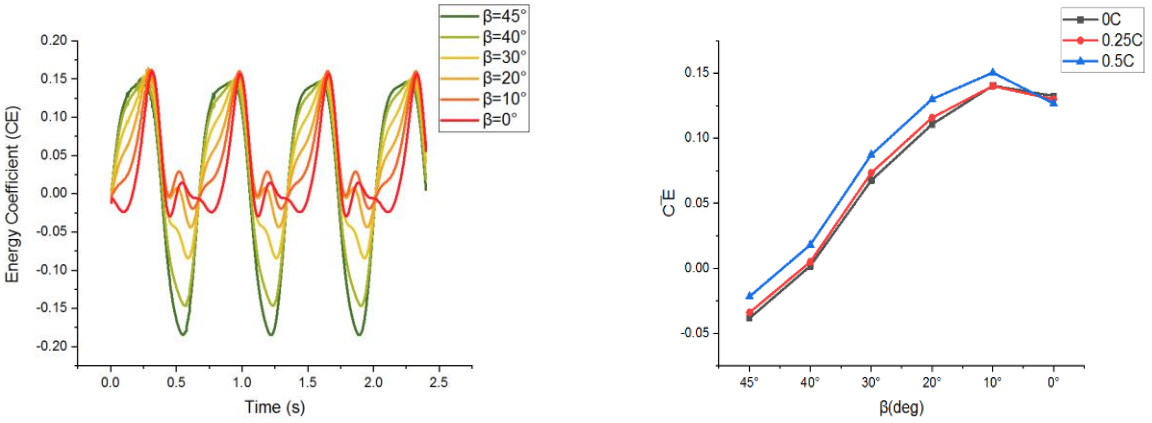

(c) (d)

Fig. 7. (a) The time history of energy coefficient (E_C) for the cases of $\beta = 45°, 40°, 30°, 20°, 10°$ and $0°$ at the rotation axis $0.25c$ (b) The time history of energy coefficient (E_C) for the cases of $\beta = 45°, 40°, 30°, 20°, 10°$ and $0°$ at the rotation axis $0.5c$ (c) The time history of energy coefficient (E_C) for the cases of $\beta = 45°, 40°, 30°, 20°, 10°$ and $0°$ at the rotation axis $0.25c$ (d) Average energy coefficient $\overline{(E_C)}$ as a function of β for different axis of rotation at 0.5c, 0.25c and 0c

However, $\text{Figure } 7(\text{a})$ shows that there are portions of the flapping motion cycle of the NACA0012 profile where energy is supplied to the profile $(E_C > 0)$, and parts of the cycle where energy is taken away from the profile $(E_C < 0)$,and it can be seen that with the increase of β, the maximum energy transfer coefficient E_{Cmax} increases slightly with closer values and the minimum energy transfer coefficient E_{Cmin} increases significantly, this means that β has little effect on the maximum peaks of the energy transfer coefficient and has great effect on the minimum peaks of the energy transfer coefficient, Moreover it was noticed that the case in which $\beta = 20°,10°$ and $0°$ had two maximum and minimum peaks ,which appeared almost at the same time, this indicates that β has a great effect on the energy transfer coefficient (E_C) during this motion especially on the cases of $\beta = 20°,10°$ and $0°$.

The effects of β on CE_{max} and CE_{min} are presented in Table 5, which shows that the variation of the coefficient CE_{min} is higher than the variation of CE_{max}.

Table 5
Summary of the effect of β on the maximum and minimum energy coefficients

Energy coefficient	β =45°	40°	30°.	20°.	10°	0°
CE_{max}	0.14971	0.15142	0.15753	0.15967	0.15991	0.15554
CE_{min}	-0.18368	-0.14648	-0.0842	-0.04379	-0.01962	-0.02558

Figures 7(a)-(c) represent the energy transfer coefficient (E_C) for the rotational axes at $0.25c$,$0.5c$ and $0c$ respectively, these results are obtained just to study the effect of the variation of the wing rotation axis on the energy transfer coefficient (E_C) under the variation of the plane β , we find that the traces of the energy transfer coefficient(E_C) $(\text{Figures } 2(\text{a}) - (\text{c}))$ for the rotation axes at $0.25c$, $0.5c$ and $0c$ respectively shows the same trend and similar behavior as well as the variation of the energy transfer coefficient (E_C) for the rotation axes at $0.25c$ and $0c$ is almost identical, but the variation of the energy transfer coefficient (E_C) for the rotation axis at $0.5c$ was higher than that of the last two axes, this indicates that the effect of the rotation axis at $0.5c$ on the variation of the energy transfer coefficient (E_C) is quite obvious than that of the two rotation axes at $0.25c$ and $0c$ as can be seen from the Table 6.

Table 6
Summary of the effect of β on the maximum and minimum energy coefficients for the rotational axes at $0.5c$ and $0c$

Energy coefficient		β =45°	40°	30°	20°	10°	0°
Axis of rotation:	CE_{max}	0.15839	0.16093	0.16609	0.17019	0.16807	0.15404
0.5*c*	CE_{min}	-0.1801	-0.14286	-0.07879	-0.04003	-0.01757	-0.0273
Axis of rotation:	CE_{max}	0.14647	0.14823	0.15196	0.15453	0.16000	0.15656
0*c*	CE_{min}	-0.18483	-0.14648	-0.08435	-0.04373	-0.01954	-0.02408

The time-averaged energy transfer (E_C) is shown in Figure 7(c). Obviously, it was observed from this figure that the average energy coefficient $\overline{(E_C)}$ in all cases of β = 45°, 40°, 30°, 20°,10° and 0° with the three-rotation axis 0.25c, 0.5c and 0c is completely positive, but it is negative for the plane β = 45°. It is also observed in this plot that the average energy transfer coefficient $\overline{(E_C)}$ for the three rotation axis increases gradually with the decrease of β and reaches a maximum value until the value of β = 10°,so from these results and those of the first case where β varies between 90° and 50° , it was noticed that the average energy coefficient $\overline{(E_C)}$ decreases significantly with the decrease of β until reaching the angle β = 70°and starts to increase strongly reaching its greatest value at β = 10°, moreover the net energy transfer to the wing is negative (energy is taken away from the airfoil) for the case of β = 90°, 80°, 70°,60°, 50° and 45° and becomes positive (energy is supplied to the airfoil) for the case of β = 40°, 30°, 20°,10° and 0°.

*3.2 The Effect of Re and Δα on the Energy Coefficient for Planes (*B*=10° And* B*=90°)*

Figures 8(a) and (b) shows the energy coefficient (E_C) versus time for two cases of β (β = 10° and β = 90°) corresponding to several Reynolds numbers: (Re=1.35.10^5, $Re = 1.93.10^5$, $Re = 3.85.10^5$, $Re = 7.72.10^5$,$Re = 10.10^5$, $Re = 13.5.10^5$) at the 0.25c rotation axis. It is clear from this figure that the hysteresis curves of the energy coefficients decrease by increasing the Reynolds number for both cases of β (β = 10° and β = 90°), which means that the variation of Reynolds number R_e has a more significant effect on the energy consumption.

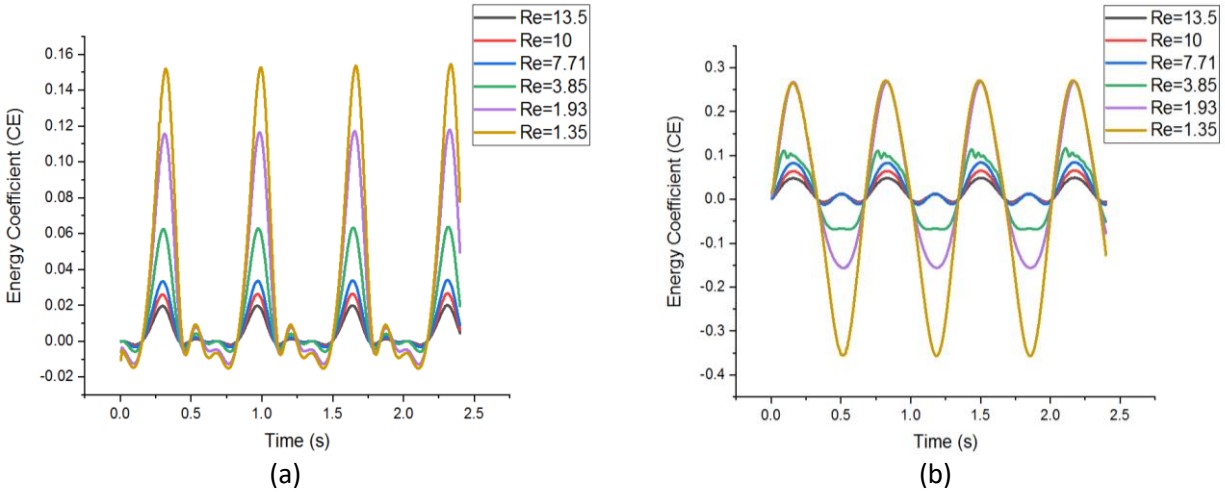

Fig. 8. (a) The time history of energy coefficient (E_C) for different Reynolds numbers at β = 10° (b) The time history of energy coefficient (E_C) for different Reynolds numbers at β = 90°

The effect of oscillation amplitude (Δα) which varies from 15° to 40° with an interval of 5° on the energy consumption is studied in this section as shown in Figures 9(a) and (b), for the two cases

of β ($\beta = 10°$ and $\beta = 90°$), at *Re*=1.35.10^5 and rotation axis 0.25c, it can be seen from this figure that the oscillation amplitude ($\Delta\alpha$) influences the maximum and minimum peaks of the coefficient energy coefficient (E_C) of the hovering wing differently under different planes β. For the plane $\beta = 10°$, there are two maximum peaks and two minimum peaks during the upstroke and down stroke of the wing, in which a minimum peak of the energy coefficient is higher than that of the maximum peaks.

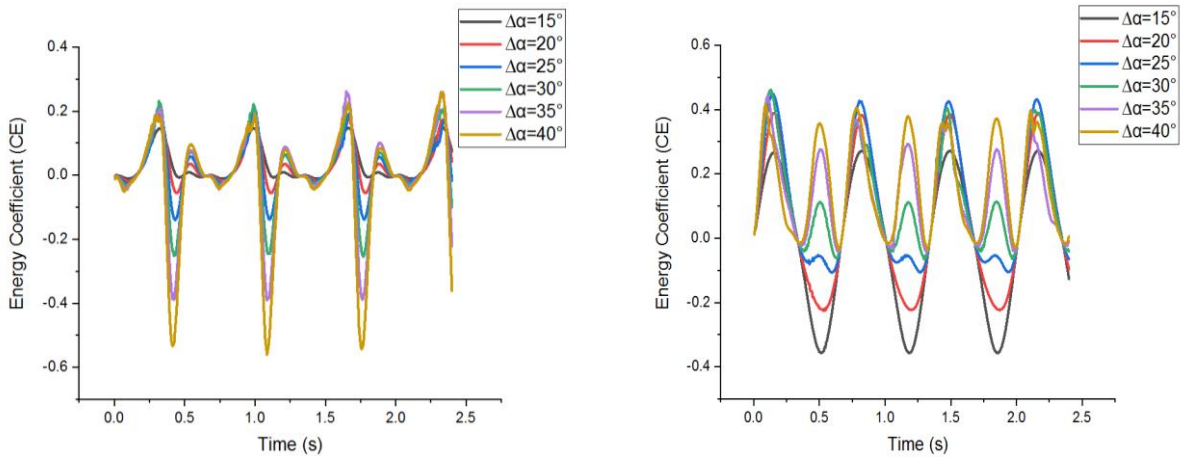

Fig. 9. (a) The time history of energy coefficient (E_C) for different oscillation amplitudes at $\beta = 10°$ (b) The time history of energy coefficient (E_C) for different oscillation amplitudes at $\beta = 90°$

On the other hand, for the plane $\beta = 90°$, it is observed that there is one maximum and one minimum peak for the oscillation amplitudes ($\Delta\alpha = 15°$ and $\Delta\alpha = 20°$) and two maximum and minimum peaks for the other oscillation amplitudes ($\Delta\alpha = 25°$,$\Delta\alpha = 30°$,$\Delta\alpha = 35°$ and $\Delta\alpha = 40°$), this new peak is induced by a large vortex that started to form inside the NACA0012 profile during the down stroke. Obviously, it is important to note that the increasing oscillation amplitude ($\Delta\alpha$) affects the energy consumption of the NACA0012 profile during the translational and rotational motion with the variation of the plane β.

3.3 The Effect of Δα on Vortex Structures and Profile Pressure for Two Planes ($\beta = 10°$ And $\beta = 90°$)

Figures 10 and 11 shows the vorticity and pressure contours respectively for two cases of the plane β, one corresponding to the plane $\beta = 10°$, and another corresponding to $\beta = 90°$ at the rotation axis $0.25c$ for different angles of attack of the upstroke motion ($\alpha = 14.96°$, $\alpha = 21.19°$) and the down stroke motion ($\alpha = 04.98°$, $\alpha = -04.99°$) with Reynolds number Re =1.35.10^5. In all cases of β, using two oscillation amplitudes ($\Delta\alpha = 15°$, $\Delta\alpha = 30°$), we will study the effect of oscillation amplitude on the vorticity and pressure contour fields.

The rotation of the aerodynamic profile during translation at the oscillation amplitude($\Delta\alpha = 15°$) (Figure 10.) leads to the beginning of the formation of leading and trailing edge vortices (LEV and TEV) in the upstroke, and no formation of vortices in the down stroke concerning the case of $\beta = 10°$, while the second case of $\beta = 90°$, the leading and trailing edge vortices (LEV and TEV) are not clear and distinct and the flow remains fully attached to the profile in the upstroke and down stroke. This is due to the fact that the angle of oscillation amplitude ($\Delta\alpha = 15°$)is not sufficient for the formation of vortices for the case of $\beta = 90°$, unlike the first case of $\beta = 10°$. From comparison between these two cases, it is observed that the variation of the inclined stroke plane had a more significant effect on the forces and vorticity fields, as can be observed in these contours(Figure 10).

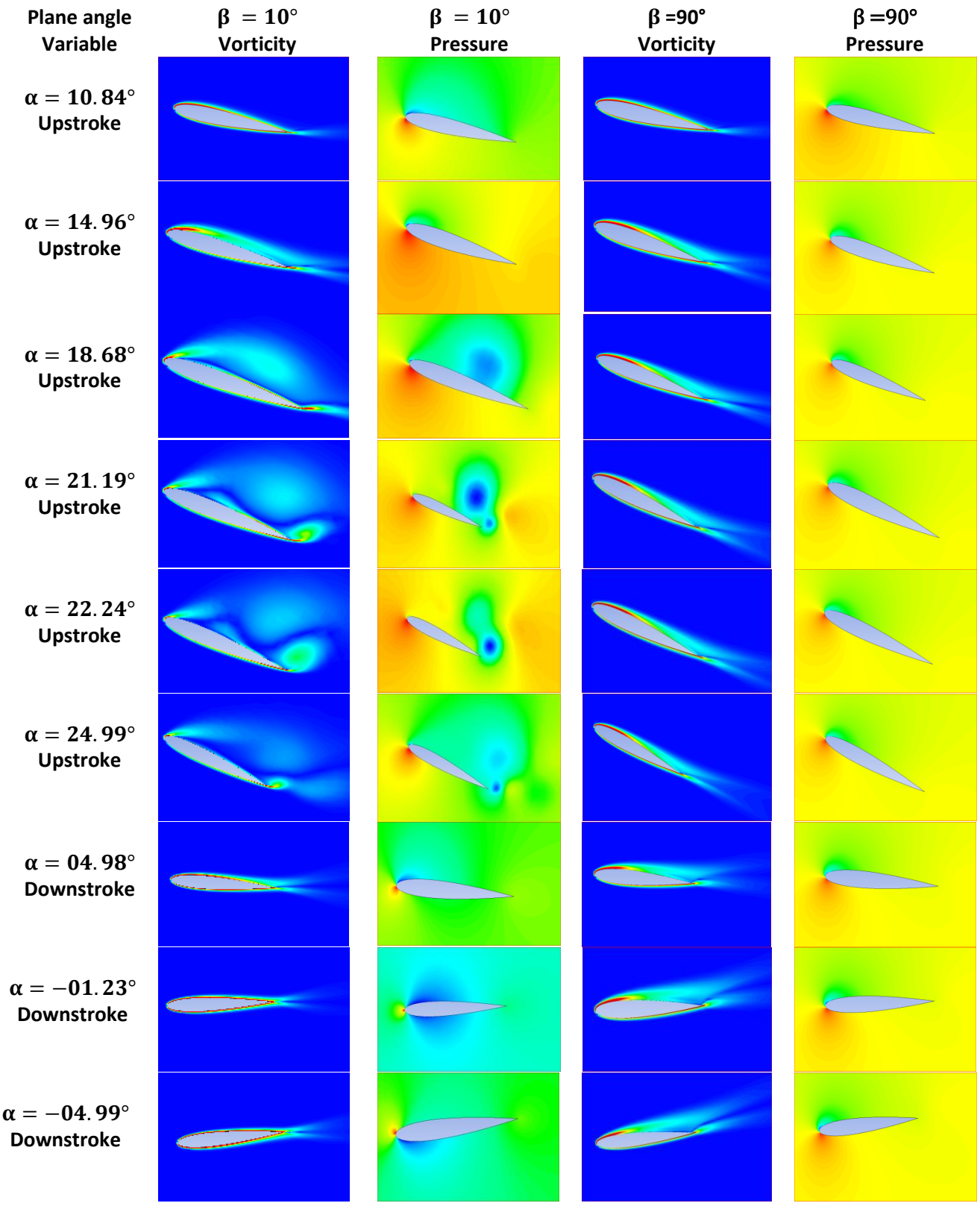

Fig. 10. Vorticity and pressure contours respectively for two cases from the plane β (β = 10° and β = 90°) at the oscillation amplitude (Δα = 15°).

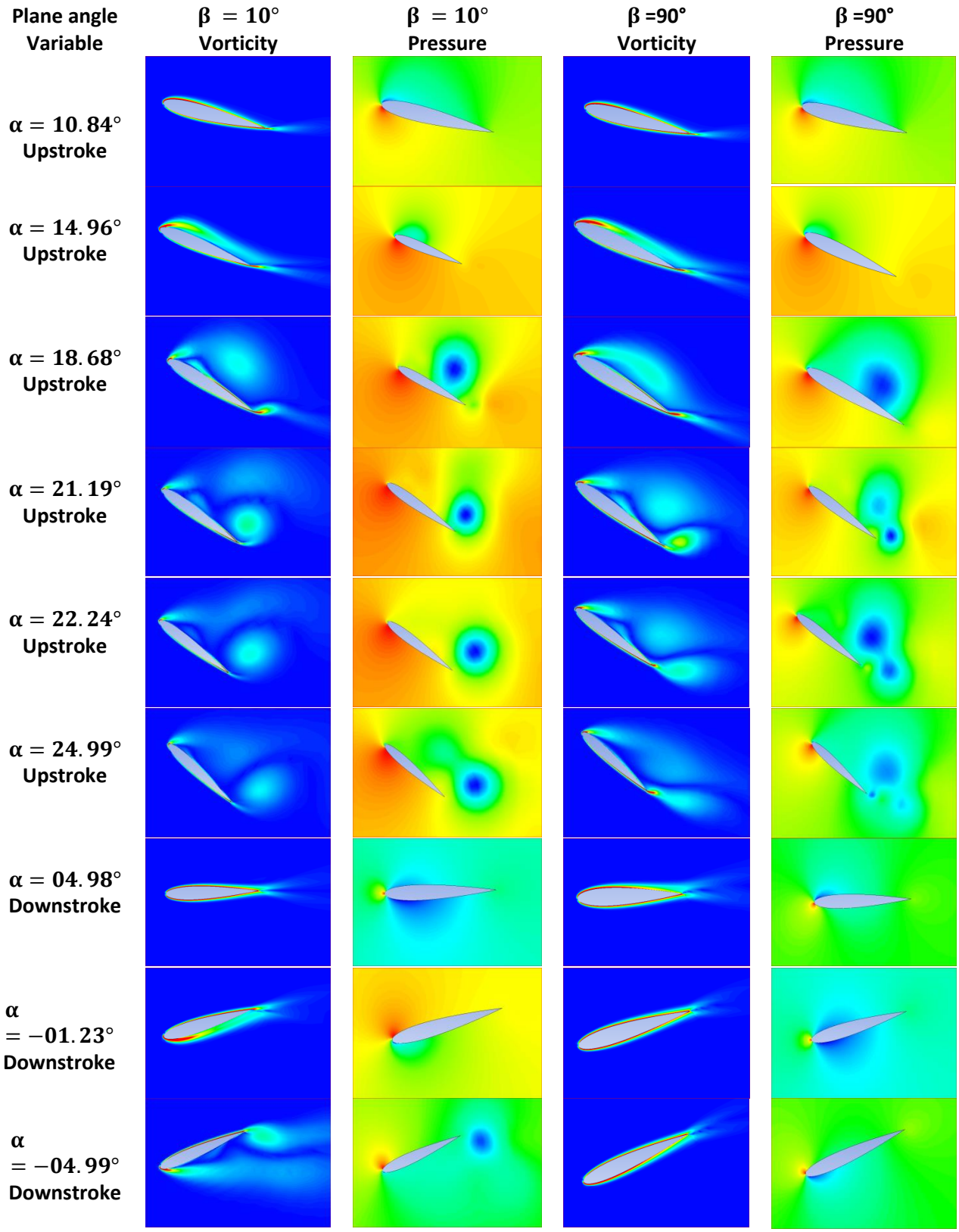

Fig. 11. Vorticity and pressure contours respectively for two cases from the plane β (β = 10° and β = 90°) at the oscillation amplitude (Δα = 30°).

The pressure distribution (Figure 10), which shows that in the first case where β = 10°, corresponding to the upstroke, there is a region of high pressure at the leading edge of the lower part of the airfoil undergoes a decrease in flow velocity and also there is a region of low pressure at

the upper surface with a stall phenomenon which will be generated in this part, while for the down stroke, the pressure decreases in the lower and upper part of the airfoil.

In the second case of $\beta = 90°$ (Figure 10), there is a region of high pressure at the leading edge of the lower part of the airfoil with a relatively low pressure at the upper part of the airfoil, this explains the highest peaks of the lift coefficient at the plane $\beta = 90°$.

For the amplitude of oscillations ($\Delta\alpha = 30°$) (Figure 11) it is observed that the flow structures at different stages of leading edge and trailing edge vortex development (LEV and TEV) in the upstroke and down stroke are very large and clear compared to the oscillation amplitude ($\Delta\alpha = 15°$), which indicates that the variation of oscillation amplitude ($\Delta\alpha$) has a more significant effect on the vorticity and pressure fields with the variation of stroke plane β.

4. Conclusions

Two-dimensional numerical simulations using $Ansys\ Fluent$ commercial software were performed for a flapping NACA0012 airfoil in hovering flight. These numerical simulations have been carried out in order to study the effect of varying the angle plane β on the aerodynamic performance of a flapping NACA0012 airfoil (Aerodynamic forces, energy consumption and wing flow structures). Furthermore, the goal of this work is to study the effect of other kinematic parameters such as oscillation amplitude ($\Delta\alpha$) and Reynolds number on the energy consumption of a NACA0012 profile during flapping motion under plane β change. The obtained numerical results were compared with the experimental data of Lee and Gerontakos [3]. This comparison revealed that numerical results are in agreement with the experimental results for lift and drag coefficients. Furthermore, the results obtained show that the change in translation plane β has a significant influence on the aerodynamic characteristics of the profile during flapping motion and on the flow fields, and from these results it is observed that a relatively large increase in the energy coefficient with the increase of the plane β, in addition, the change of the rotation axis slightly influences on the energy coefficient with the change of the plane β, as it can be seen that the maximum energy coefficient E_{Cmax} is obtained for the plane $\beta = 90°$ and the minimum energy coefficient E_{Cmin} is obtained at $\beta = 10°$, on the other hand, the maximum average energy coefficient is obtained at $\beta = 10°$ and the minimum average coefficient is obtained at $\beta = 70°$ which indicates that the variation of the plane β has a significant effect on the energy coefficient (E_C) and the average energy coefficient $\overline{(E_C)}$.

The increase of Reynolds number Re and oscillation amplitude ($\Delta\alpha$) also influence on the energy coefficient with the variation of plane β in which, the energy coefficient decreases by the increase of Reynolds number Re and increases by the increase of oscillation amplitude ($\Delta\alpha$), and it is also found that the change of Reynolds number Re and oscillation amplitude ($\Delta\alpha$) have a significant impact on the flow structures and vortex development.

References

[1] Nor Elyana Ahmad, Essam Abo-Serie, and Adrian Gaylard. "Mesh Optimization for Ground Vehicle Aerodynamics." *CFD Letters* 2, no.1 (2010): 54-65.

[2] Mostafa Abobaker, Sogair Addeep, Lukmon O Afolabi, Abdulhafid M Elfaghi. "Effect of Mesh Type on Numerical Computation of Aerodynamic Coefficients of NACA 0012 Airfoil." *Journal of Advanced Research in Fluid Mechanics and Thermal Sciences* 87, no. 3 (2021): 31-39. https://doi.org/10.37934/arfmts.87.3.3139

[3] Bassam Amer Abdulameer Shlash1, and Ibrahim Koç. "Turbulent Fluid Flow and Heat Transfer Enhancement Using Novel Vortex Generator." *Journal of Advanced Research in Fluid Mechanics and Thermal Sciences* 96, no. 1 (2022): 36-52. https://doi.org/10.37934/arfmts.96.1.3652

[4] Fatin Alias, Mohd Hairil Mohd, Mohd Azlan Musa, Erwan Hafizi Kasiman, and Mohd Asamudin A Rahman. "Flow Past a Fixed and Freely Vibrating Drilling Riser System with Auxiliaries in Laminar Flow." *Journal of Advanced*

Research in Fluid Mechanics and Thermal Sciences 87, no. 3 (2021): 94-104. https://doi.org/10.37934/arfmts.87.3.94104

[5] Wernert, Philippe, Wolfgang Geissler, Markus Raffel, and Juergen Kompenhans. "Experimental and numerical investigations of dynamic stall on a pitching airfoil." *AIAA journal* 34, no. 5 (1996): 982-989. https://doi.org/10.2514/3.13177

[6] Anderson, Jamie M., K. Streitlien, D. S. Barrett, and Michael S. Triantafyllou. "Oscillating foils of high propulsive efficiency." *Journal of Fluid mechanics* 360 (1998): 41-72. https://doi.org/10.1017/S0022112097008392

[7] Lee, T., and P. Gerontakos. "Investigation of flow over an oscillating airfoil." *Journal of Fluid Mechanics* 512 (2004): 313-341. https://doi.org/10.1017/S0022112004009851

[8] Wang, Shengyi, Derek B. Ingham, Lin Ma, Mohamed Pourkashanian, and Zhi Tao. "Numerical investigations on dynamic stall of low Reynolds number flow around oscillating airfoils." *Computers & fluids* 39, no. 9 (2010): 1529-1541. https://doi.org/10.1016/j.compfluid.2010.05.004

[9] Amiralaei, Mohammadreza. "Computational fluid dynamic simulation of airfoils in unsteady low Reynolds number flows." *USA: Defense Technical Information Center, DTIC* (2012).

[10] Amiralaei, M. R., H. Alighanbari, and S. M. Hashemi. "An investigation into the effects of unsteady parameters on the aerodynamics of a low Reynolds number pitching airfoil." *Journal of Fluids and Structures* 26, no. 6 (2010): 979-993. https://doi.org/10.1016/j.jfluidstructs.2010.06.004

[11] Amiralaei, M. R., H. Alighanbari, and S. M. Hashemi. "Flow field characteristics study of a flapping airfoil using computational fluid dynamics." *Journal of Fluids and Structures* 27, no. 7 (2011): 1068-1085. https://doi.org/10.1016/j.jfluidstructs.2011.06.005

[12] Bhat, Shantanu S., and Raghuraman N. Govardhan. "Stall flutter of NACA 0012 airfoil at low Reynolds numbers." *Journal of Fluids and Structures* 41 (2013): 166-174. https://doi.org/10.1016/j.jfluidstructs.2013.04.001

[13] Liu, Jian, HaiSheng Sun, Yong Huang, Yong Jiang, and ZhiXiang Xiao. "Numerical investigation of an advanced aircraft model during pitching motion at high incidence." *Science China Technological Sciences* 59, no. 2 (2016): 276-288. https://doi.org/10.1007/s11431-015-5957-2

[14] Zakaria, M. Y., F. Jafari, and M. R. Hajj. "Flow measurements associated with lift enhancement of a plunging airfoil oscillating at high angles of attack and reduced frequencies." In *Proc., 32nd AIAA Aerodynamic Measurement Technology and Ground Testing Conf., AIAA 2016*, vol. 3401. 2016. https://doi.org/10.2514/6.2016-3401

[15] Zakaria, M. Y., H. E. Taha, and M. R. Hajj. "Measurement and modeling of lift enhancement on plunging airfoils: A frequency response approach." *Journal of Fluids and Structures* 69 (2017): 187-208. https://doi.org/10.1016/j.jfluidstructs.2016.12.004

[16] Sun, Mao, and Jian Tang. "Unsteady aerodynamic force generation by a model fruit fly wing in flapping motion." *Journal of experimental biology* 205, no. 1 (2002): 55-70. https://doi.org/10.1242/jeb.205.1.55

[17] Wang, Z. Jane, James M. Birch, and Michael H. Dickinson. "Unsteady forces and flows in low Reynolds number hovering flight: two-dimensional computations vs robotic wing experiments." *Journal of Experimental Biology* 207, no. 3 (2004): 449-460. https://doi.org/10.1242/jeb.00739

[18] Meile, Walter, Günter Brenn, Aaron Reppenhagen, Bernhard Lechner, and Anton Fuchs. "Experiments and numerical simulations on the aerodynamics of the Ahmed body." *CFD letters* 3, no. 1 (2011): 32-39.

[19] Wang, Z. Jane. "Two dimensional mechanism for insect hovering." *Physical review letters* 85, no. 10 (2000): 2216. https://doi.org/10.1103/PhysRevLett.85.2216

[20] Yu, Yongliang, and Binggang Tong. "A flow control mechanism in wing flapping with stroke asymmetry during insect forward flight." *Acta Mechanica Sinica* 21, no. 3 (2005): 218-227. https://doi.org/10.1007/s10409-005-0032-z

[21] Gao, Tong, and Xi-Yun Lu. "Insect normal hovering flight in ground effect." *Physics of Fluids* 20, no. 8 (2008): 087101. https://doi.org/10.1063/1.2958318

[22] Jardin, Thierry, Laurent David, and Alain Farcy. "Characterization of vortical structures and loads based on time-resolved PIV for asymmetric hovering flapping flight." In *Animal Locomotion*, pp. 285-295. Springer, Berlin, Heidelberg, 2010. https://doi.org/10.1007/978-3-642-11633-9_23

[23] Sudhakar, Y., and S. Vengadesan. "Flight force production by flapping insect wings in inclined stroke plane kinematics." *Computers & Fluids* 39, no. 4 (2010): 683-695. https://doi.org/10.1016/j.compfluid.2009.11.004

[24] Shanmugam, A. R., and C. H. Sohn. "Systematic investigation of a flapping wing in inclined stroke-plane hovering." *Journal of the Brazilian Society of Mechanical Sciences and Engineering* 41, no. 8 (2019): 1-16. https://doi.org/10.1007/s40430-019-1840-6

[25] Muhammad Qamaran Abdul Aziz, Juferi Idris, and Muhammad Firdaus Abdullah. "Simulation of the Conical Gravitational Water Vortex Turbine (GWVT) Design in Producing Optimum Force for Energy Production." *Journal of*

Advanced Research in Fluid Mechanics and Thermal Sciences 89, no. 2 (2022): 99-113. https://doi.org/10.37934/arfmts.89.2.99113

[26] Rival, D., G. Hass, and C. Tropea. "Recovery of energy from leading- and trailing-edge vortices in tandem-airfoil configurations." *Journal of Aircraft* 48, no. 1 (2011): 203–211. https://doi.org/10.2514/1.C031062